THE JOURNAL OF PHYSICAL CHEMISTRY B

ARTICLE

pubs.acs.org/JPCB

Structure and Thermodynamics of Amylin Dimer Studied by Hamiltonian-Temperature Replica Exchange Molecular Dynamics Simulations

Rozita Laghaei,*,† Normand Mousseau,*,† and Guanghong Wei‡

†Département de Physique and Groupe de Recherche sur les Protéines Membranaires (GEPROM), Université de Montréal, C.P. 6128, succursale Centre-ville, Montréal (Québec), Canada

‡State Key Laboratory of Surface Physics, Key Laboratory for Computational Physical Sciences (Ministry of Education), and Department of Physics, Fudan University, 220 Handan Road, Shanghai 200433, China

ABSTRACT: The loss of the insulin-producing β-cells in the pancreatic islets of Langerhans, responsible for type-II diabetes, is associated with islet amyloid deposits. The main component of these deposits is the amyloid fibrils formed by the 37-residue human islet amyloid polypeptide (hIAPP also known as amylin). Although the fibrils are well characterized by cross β structure, the structure of the transient oligomers formed in the early stage of aggregation remains elusive. In this study, we apply the Hamiltonian-temperature replica exchange molecular dynamics to characterize the structure and thermodynamics of a full-length hIAPP dimer in both the presence and the absence of the Cys2−Cys7 disulfide bond. We compare these results with those obtained on the monomeric and dimeric forms of rat IAPP (rIAPP) with a disulfide bridge which differ from the hIAPP by 6 amino acids in the C-terminal region, but it is unable to form fibrils. Using a coarse-grained protein force field (OPEP—the Optimized Potential for Efficient peptide structure Prediction) running for a total of 10−28 μs per system studied, we show that sequences sample α-helical structure in the N-terminal region but that the length of this secondary element is shorter and less stable for the chains without the disulfide bridge (residues 5−16 for hIAPP with the bridge vs 10−16 for hIAPP without the bridge). This α-helix is known to be an important transient stage in the formation of oligomers. In the C-terminal, the amyloidogenic region of hIAPP, β-strands are seen for residues 17−26 and 30−35. On the contrary, no significant β-sheet content in the C-terminal is observed for either the monomeric or the dimeric rIAPP. These numerical results are fully consistent with recent experimental findings that the N-terminal residues are not part of the fibril by forming α-helical structure but rather play a significant role in stabilizing the amyloidogenic region available for the fibrillation.

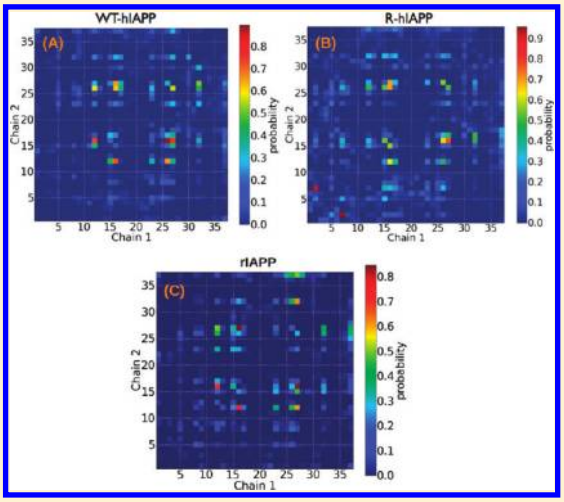

I. INTRODUCTION

Amyloid deposits of human islet amyloid polypeptide (hIAPP, or amylin) are almost always present in type-II diabetes patients' β-cells. It was shown that hIAPP, a 37-amino acid protein with a disulfide bond at the Cys2−Cys7 position and an amidated C-terminal[1] of sequence KCNTATCATQRLANFLVHSSNNF-GAILSSTNVGSNTY, forms aggregates causing β-cell death, followed by a reduction in insulin production.[2] Not surprisingly, in view of its importance, the aggregation process of hIAPP has been the subject of a number of experimental and theoretical studies over the past decade.[3−15] In spite of these efforts, however, a detailed understanding of the first steps of aggregation is still missing. In particular, little is known about the structure of low molecular weight oligomers formed in the prefibrillar stage. Recent experiments provided evidence for the occurrence of α-helical intermediates of hIAPP in the presence of membrane[16] and the helix−helix association in the lag phase of aggregation.[17] NMR studies have shown that hIAPP has a strong preference for an α-helical secondary structure near the N-terminal region of the peptide in solution.[18,19] Consistent with these experimental results, our recent molecular dynamics simulations study probed a partial α-helical structure in the N-terminal region of the hIAPP monomer.[20] A number of studies have suggested that the aggregation of hIAPP takes place after the peptide is anchored on a membrane by an N-terminal α-helix. Brender et al.,[7] for example, showed that membrane disruption and amyloid formation are two separate processes that happen in different regions of hIAPP. Liposome leakage experiments on full-length hIAPP and $hIAPP_{1-19}$ fragments at low concentration confirmed that the pathological membrane-disrupting activity comes from the IAPP N-terminal region as both sequences induce almost identical

Received: September 16, 2010
Revised: February 8, 2011
Published: March 08, 2011

disruption in membrane even though, at higher concentration, only full-length hIAPP forms amyloid fibers. Understanding the role of the α-helical form in hIAPP aggregation, both as an important structural element in the N-terminal to ease insertion into the membrane and as a precursor for the formation of oligomers in the amyloidogenic region, is therefore crucial.[16,21−24] Experimental studies also show that the presence of a disulfide bridge at position Cys2−Cys7 prevents the N-terminal from adopting β-strand conformations, stabilizing the α-helical structure necessary for anchoring to the membrane. Contrary to what could be expected, it seems that its presence accelerates the aggregation process.[4,25,26]

It is interesting to further compare hIAPP with the rat sequence. The rat IAPP (rIAPP), which differs from the human sequence by only 6 residues positioned in the protein's central section—three prolines at positions 25, 28, and 29 and H18R, L23F, and V26I—is not toxic. The nontoxicity of rIAPP has usually been attributed to its inability to form the β-sheet amyloid aggregates. Experiments suggested that rat and human IAPP interact similarly with lipid monolayers,[22] and it is therefore thought that the two peptides may have several common structural features. High-resolution NMR studies show that rIAPP adopts an α-helical structure spanning residues 5−19.[27] Using solution NMR spectroscopy, Nanga et al.[28] studied the 3D structure of rIAPP in the presence of a membrane suggesting that the α-helix region plays a crucial role in the self-association. Rat IAPP shows helical structure spanning residues 5−23 with a distortion at residues 18 and 19, and the C-terminal remains disordered. However, the peptide is exposed to the water, whereas $hIAPP_{1-19}$ is buried within the micelle. Interestingly, protonation of His18 of $hIAPP_{1-19}$ drives the peptide to the surface of the membrane and decreases its toxicity.[29,30]

To better understand the role of the disulfide bridge and the amino acid sequence on the early stage of aggregation in solution, we study the full-length hIAPP dimer, with and without the disulfide bridge, and compare its conformational properties with that of the monomer, already studied by us,[20] as well as with rIAPP in both monomeric and dimeric forms. The simulations are performed by Hamiltonian-temperature replica exchange molecular dynamics (HT-REMD) which is a modified version of the temperature REMD (T-REMD) method,[31] combined with a coarse-grained protein force field (OPEP—the Optimized Potential for Efficient peptide structure Prediction).[32]

II. METHODS

We study the structure and thermodynamics of the hIAPP dimer and of the rIAPP monomer and dimer using our in-house software package . The amino acid sequence of rIAPP is KCNTATCATQRLANFLVRSSNNLGPVLPPTNVGSNTY, where the mutations with respect to the human form are underlined. hIAPP is constructed in two forms, the C-amidated with a disulfide bridge between residues Cys2−Cys7 (wild-type or WT-hIAPP) and without (reduced form, R-hIAPP). The intra- and interpeptide interactions are described using the coarse-grained force field OPEP version 3.2.[32] In this force field, amino acids are represented by all the heavy backbone atoms, Cα, N, C, and O, as well as the amine hydrogen H and a single centroid for the side chains of the amino acids except the proline which is represented by all heavy atoms. OPEP's parameters are described in detail in refs 32 and 33. OPEP version 3.2 is a nonbiased potential that has been shown to predict correctly the structural and thermodynamical properties of a number of proteins with various degree of α-helix and β-sheet secondary structures.[13,20,34−39]

HT-REMD is shown to accelerate sampling noticeably to fully converged thermodynamical sampling compared with T-REMD[20] and designed to facilitate configurational sampling for large systems. These systems are dominated by states with lower entropy where increasing temperature in T-REMD does not significantly help the reversible exploration of folding pathways.[40] A detailed discussion about the advantages of HT-REMD over standard T-REMD is presented in ref 20.

We use the following procedure: a set of N replicas are run at T different temperatures with exchange acceptance of replica i with its neighbor j as given by

$$p(i,j) = \min\left\{1.0, \exp\left[\left(\frac{1}{k_B T_i} - \frac{1}{k_B T_j}\right)(E_i - E_j)\right]\right\} \quad (1)$$

where E_i is the configurational energy of replica i, and T_i is its initial temperature. In parallel, M replicas are also run at the highest temperature but with variable attractive force strengths. This set undergoes a trial exchange similar to that of T-REMD, with

$$p(i,j) = \min\{1.0, \exp[-\beta([H_i(X') + H_j(X)] - [H_i(X) + H_j(X')])]\} \quad (2)$$

where $H_i(X')$ is the Hamiltonian of configuration X' for replica i, and X and X' are the configurations for replicas i and j, respectively.

Simulation runs are started from random conformations generated in short high-temperature MD runs. HT-REMD simulations are run using 40 replicas in all cases, with 35 temperatures ranging from 240 to 555 K and five Hamiltonian replicas run at the highest temperature (555 K) with a scaling on the attraction terms of the interactions (hydrogen bonding, hydrophobic, and Lennard-Jones) set at 0.8, 0.7, 0.6, 0.4, and 0.2 of the full-strength attraction. The peptides are placed in a 60 Å radius confining sphere with reflecting boundary conditions, and the temperature is set with an external bath with a coupling time of 500 fs.[41] The time step for all four sets is 1.5 fs. Exchanges are attempted every 15 ps, and the RATTLE algorithm is used to constrain the bond lengths.[42]

Simulations for the dimers of WT-hIAPP and R-hIAPP are run for 700 ns per replica, resulting in a cumulative simulation time of 28 μs for each system. For the rIAPP monomer and dimer, the simulation times are 400 and 250 ns, respectively. We ensure that equilibration is reached by comparing entropy curves averaged over different time intervals. The quantities presented here are all averaged over the last 200 ns of the simulations which represent a total of 26 600 conformations.

PTWHAM, the weighted histogram method adapted to Hamiltonian replica exchange, is applied for the thermodynamical analysis.[43] The secondary structure calculation is carried out using STRIDE.[44] Side chains are considered in contact if they are less than 6.5 Å apart. Entropy is calculated from subtracting free energy (F) obtained by PTWHAM and the corresponding internal energy (U) by: $\Delta S = (U - F)/T$. The free-energy landscape has been determined by the histogram analysis method for two sets of reaction coordinates, the percentage of β-sheet content and end-to-end distance, as well as the percentage of α-helix content and end-to-end distance. The last 200 ns (26 600) structures are analyzed at temperature 300 K . Clustering analysis

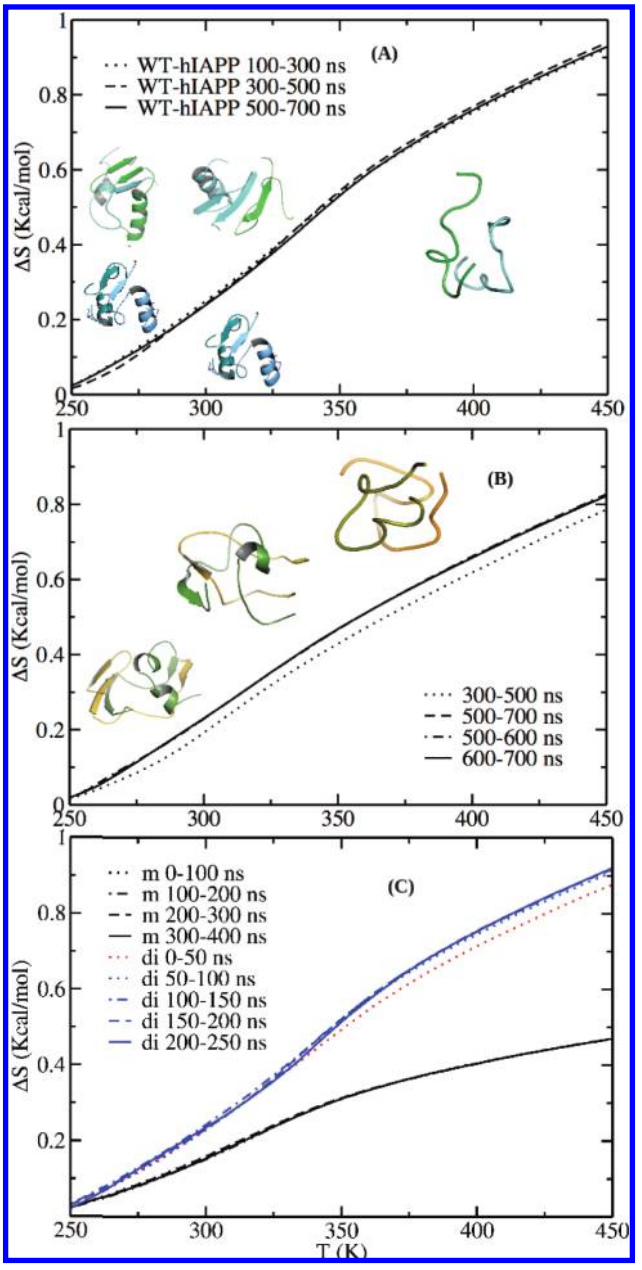

Figure 1. Convergence of the HT-REMD simulations of WT-hIAPP dimer, R-hIAPP dimer, and the monomeric and dimeric forms of rIAPP. Conformational entropy ΔS as a function of temperature calculated over the time intervals indicated in the three panels for (A) WT-hIAPP dimer, (B) R-hIAPP dimer, and (C) rIAPP monomer (mono) and dimer. Here, we report the entropy relative to its value at the lowest temperature. The structures in panel (A) from left to right are the centers of the largest clusters at 260, 300, and 400 K. Similarly, the structures in panel (B) from left to right are the centers of the largest clusters at 260 K, 300 K, and random coil at temperature higher than 350 K. As shown in the figure, both the rIAPP monomer and the dimer reach equilibration very fast.

is performed iteratively as reported in previous studies[20,45] using a C_α root-mean-square displacement (rmsd) cutoff of 2.25 Å.

III. RESULTS AND DISCUSSION

To investigate the dimeric structures formed in the early steps of hIAPP aggregation, we simulate the hIAPP dimer as well as

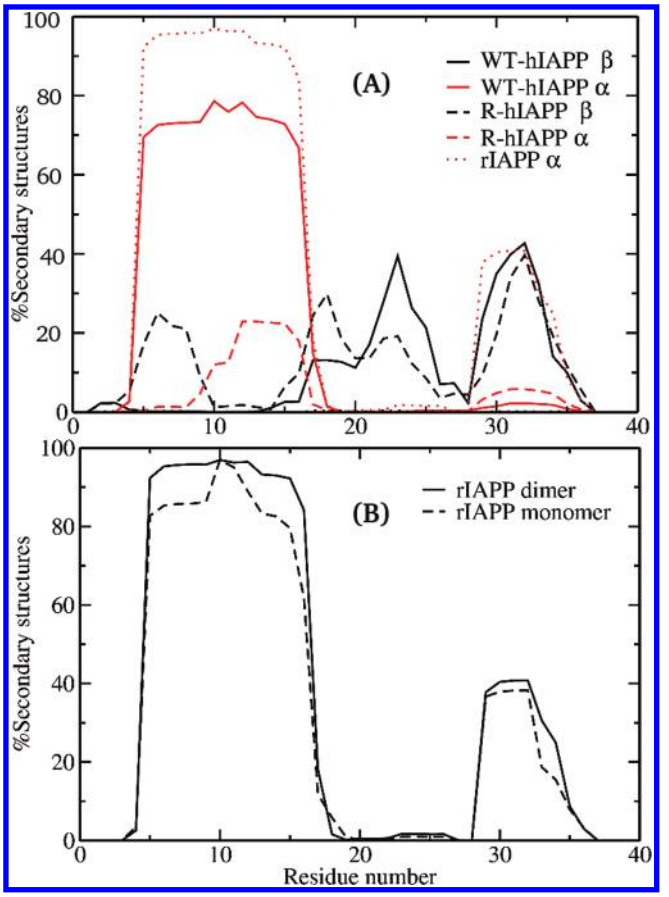

Figure 2. Propensity of the most regular secondary structure α-helix and β-sheet as a function of residue number at 300 K for: (A) dimers of WT-hIAPP and R-hIAPP and (B) rIAPP monomer and dimer. For dimers, the probability is averaged over the two chains.

rIAPP in monomeric and dimeric forms. In the following sections, we first report, in detail, results for WT-hIAPP. Results for the three other systems are then reported sequentially and compared with those of WT-hIAPP.

A. Thermodynamical Properties and Structural Characterization of the hIAPP Dimer. *1. hIAPP Dimer with a Disulfide Bridge.* Simulations for the WT-hIAPP dimer are performed starting from a random conformation as explained in the Methods section. Simulations are run for 700 ns for each replica and tested for equilibration. This is done by comparing the entropy as a function of temperature averaged over sequential time intervals. Figure 1A, for example, shows that the entropy for three consecutive 200 ns time intervals (100−300, 300−500, and 500−700 ns) is well converged and is stable over time. For ease of comparison with R-hIAPP, we restrict our statistical analysis to the last 200 ns of the simulation (also shown).

Secondary structure statistics are accumulated over the last 200 ns of the simulations (26 600 structures for each replica) at temperatures below 400 K as the percentage of the secondary structures are less than 2% at higher temperatures. Figure 2(A) shows the probability of forming α-helix or β-sheet, averaged over the two chains as a function of residue number at 300 K. Residues 5−16 show a very high propensity of forming α-helical structure (more than 75%), while residues 17−27 and 29−35 show a significant tendency to form β-sheets (up to 40%). These results compare well with NMR spectroscopic studies which find

that the N-terminal residues 5−16 have a high propensity to adopt α-helical structure at room temperature:[23] averaged over the two chains, α-helix and β-strand contents are 38% at 300 K.

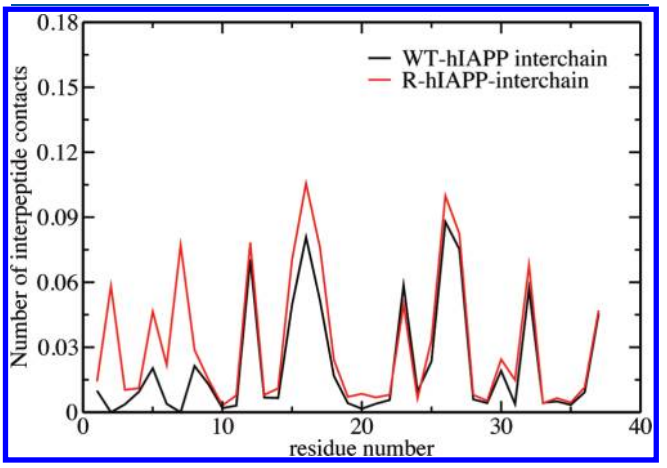

Figure 3. Average number of interpeptide side-chain−side-chain contacts as a function of residue number at 300 K for the dimers of WT-hIAPP and R-hIAPP.

The high α-helical propensity for residues 5−16 is identical with that found for the monomer in our previous study, while the situation is markedly different for the C-terminal where the monomer shows a relatively low probability of forming ordered secondary structure, with β-strand content never above 20% for residues 22−27 and 29−35 for a total percentage of secondary structure reaching only 31% at 300 K.[20] Interactions between the two chains lead to a higher propensity of 38% here. Moreover, the β-strand-rich region is broader for the dimer, extending down to Val17. These results clearly show that the dimeric form of WT-hIAPP is much more structured, especially in the C-terminal region, which is responsible for protein aggregation.

Statistics of intrachain and interchain contacts indicate that the β-sheets are mostly stabilized by the contacts between proteins. The number of the interchain contacts for each residue is presented in Figure 3. Residues Cys2 and Cys7 have zero interchain contacts as expected. In Figure 3 there are five peaks for the residues Leu12, Leu16, Phe23, Ile26−Leu27, and Val32, and the residues with the highest hydrophobicity show the highest contacts.

Our results are also compatible with solid-state NMR secondary chemical shift analysis of the amyloidogenic fragment hIAPP20−29 (SNNFGAILSS) by Nielsen[24] who revealed that

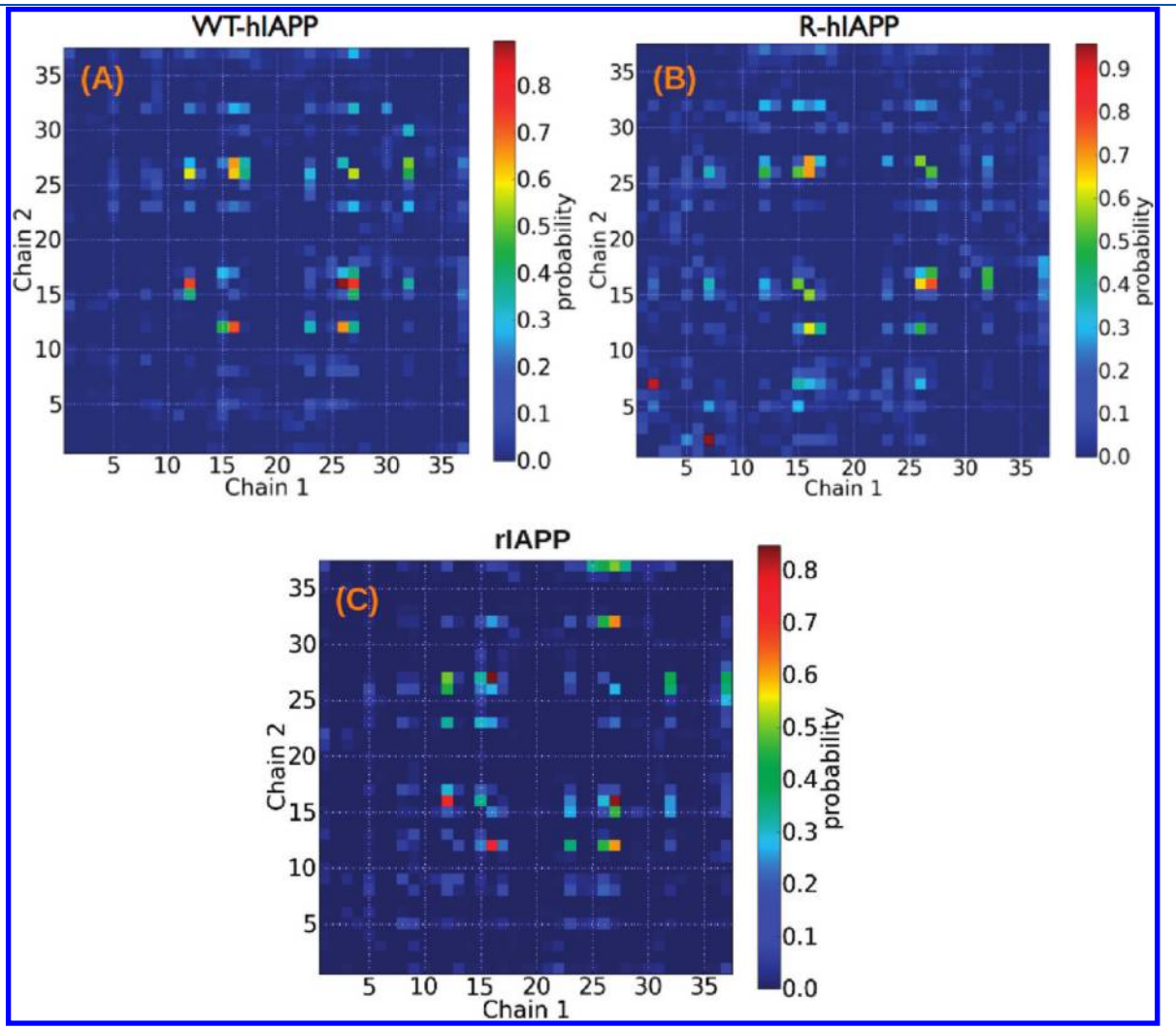

Figure 4. Interpeptide side-chain−side-chain contact map for the dimer of (A) WT-hIAPP, (B) R-hIAPP, and (C) rIAPP at 300 K. The probability of the side-chain contacts between chain 1 and chain 2 is averaged over 26 600 structures.

dx.doi.org/10.1021/jp108870q |J. Phys. Chem. B 2011, 115, 3146–3154

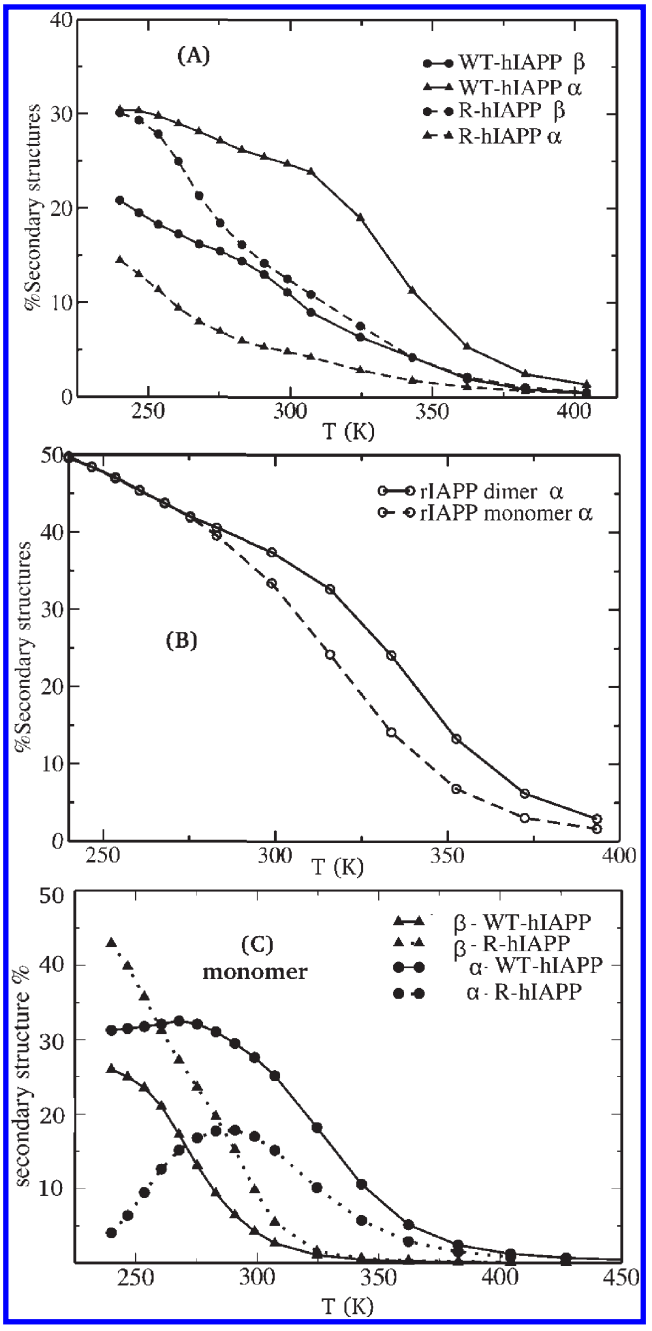

Figure 5. Secondary structure percentage as a function of temperature for (A) WT-hIAPP and R-hIAPP dimers, (B) rIAPP monomer and dimer, and (C) WT-hIAPP and R-hIAPP monomers from ref 20.

β-strand conformations for the residues 22−27 belong to the antiparallel hetero zipper class. This structure implies contacts between Leu27 and Ile26, Gly24 and Phe23, Leu27 and Phe23, and Ile26 and Phe23. This structure also shows hydrophobic interactions between side chains of Phe23 and Leu27 within the same sheet and Phe23 and Ile26 of the opposite sheet.[24] These interactions are also populated in the dimeric structure of WT-hIAPP. As seen in the interpeptide side-chain−side-chain contact probability map at 300 K in Figure 4(A), the contact probabilities between these pairs of residues are all between 20 and 56%, and the strongest contact is seen between Leu12−Leu16, Leu12−Ile26, Leu16−Ile26, and Leu16−Leu27 (average contact probability for

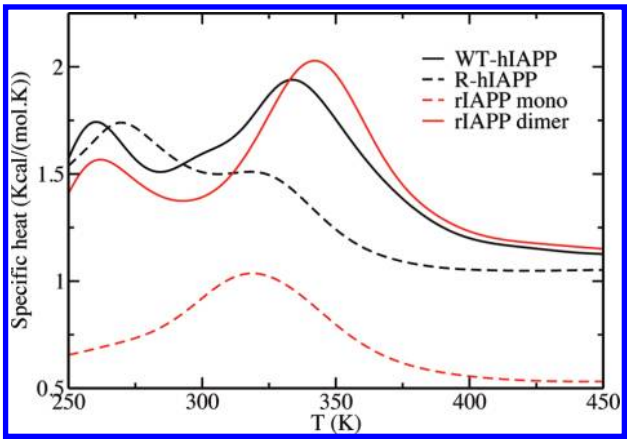

Figure 6. Specific heat curves as a function of temperature for all the systems: WT-hIAPP (dimer), R-hIAPP (dimer), rIAPP (monomer), and rIAPP (dimer).

each pair is between 66 and 90%). Another amyloidogenic region has been identified by Nilsson and Raleigh[46] who found that the residues 30−37 form ordered amyloid deposits. Interpeptide contacts between Thr30 and Val32 are seen in Figure 4(A), with probabilities of 28−35%. We also observe contacts between residue Tyr37 and residues Phe15 and Phe23, albeit with a low probability of 18−22%. These were identified by Miranker et al.[47] to be necessary for the formation of mature hIAPP fibers. More interestingly, the WT-hIAPP dimer shows strong interchain hydrophobic interactions (with contact probabilities of 40−80%) between the side chains of L12-F15 and L12-L16. These residues are located in the N-terminal region and have an ∼80% propensity to adopt helical structure (see Figure 2). This may indicate that some helix−helix association is present in the WT-hIAPP dimer.

Figure 5(A) shows the temperature dependence of α-helix and β-sheet contents for WT-hIAPP and R-hIAPP dimers. As expected, we observed a decrease in both α and β contents with increasing temperature. However, the α-helical content persists at a relatively high percentage up to 320 K. Above this temperature, the α-helical propensity drops rapidly to less than 5% by 370 K, a behavior also observed for the monomer.[20] This similarity is to be expected as there are very few interchain contacts in the N-terminal region at 370 K. The situation is different for the C-terminal: while at very low temperature, the β-sheet content for the dimeric WT-hIAPP is slightly lower than for the monomer (22 vs 26%), it is significantly more stable as the temperature rises. At 300 K, for example, the dimer shows about 10% β-sheet propensity compared to only 4% for the monomer. Even though β-sheets are not predominant at any temperature in WT-hIAPP, our simulations show that its propensity is significantly enhanced by the interchain interactions, especially near the biologically relevant temperatures.

To help understand the evolution of secondary structure as a function of temperature, we can look at the temperature dependence of the specific heat (Figure 6). We observe two peaks in the curve of WT-hIAPP around 260 and 330 K, which are typically associated with structure changes. This is confirmed by clustering analysis: the centers of the largest clusters are shown in Figure 7 (A) for temperature around the two peaks in the specific heat—240, 260, and 300 K. We observe a clear difference in the secondary structure at the first peak followed by a transition to random coil at 330 K as shown in Figure 1(A) .

dx.doi.org/10.1021/jp108870q |J. Phys. Chem. B 2011, 115, 3146–3154

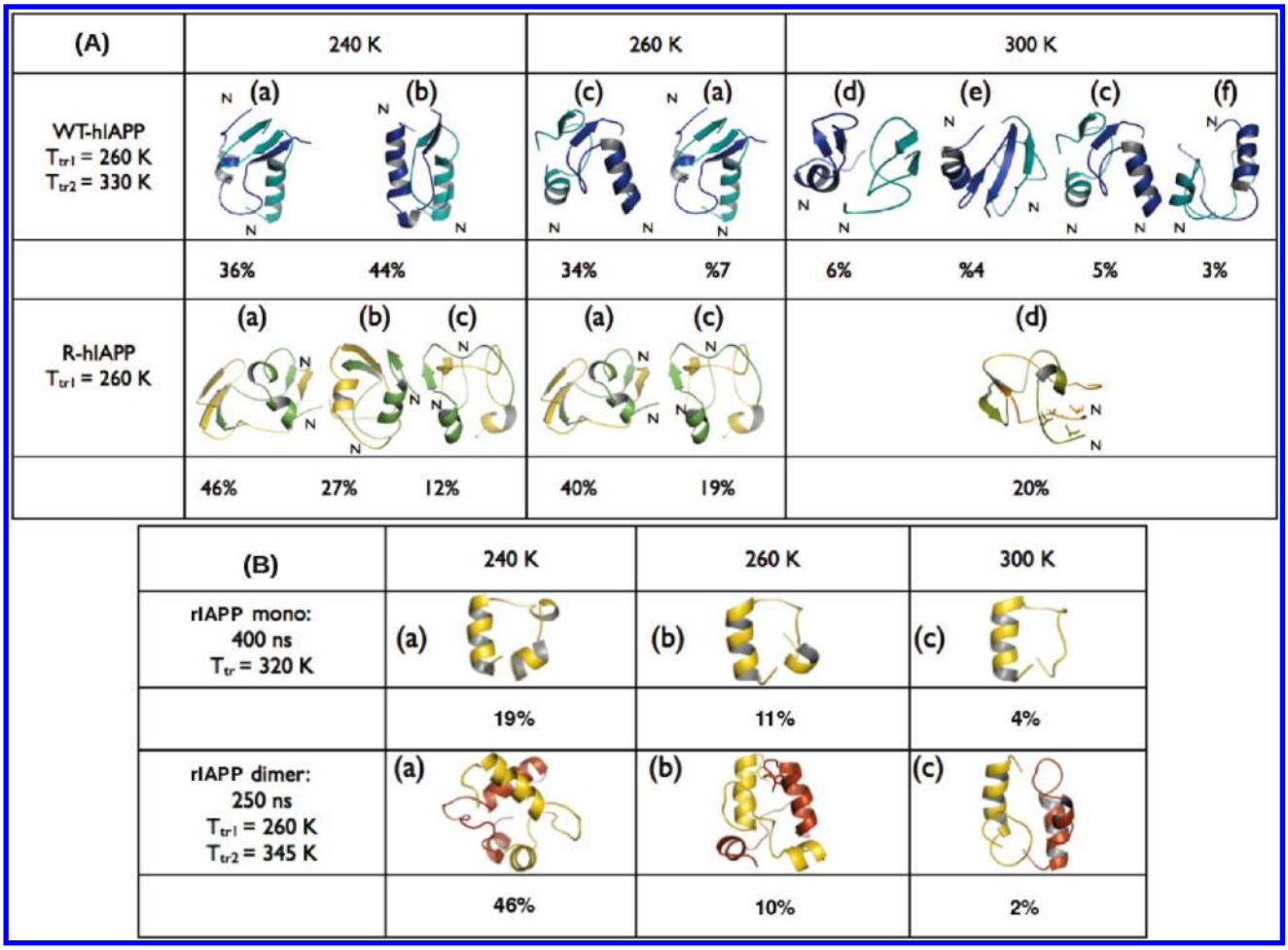

Figure 7. Centers of the largest clusters at three different temperatures (240, 260, and 300 K) for: (A) WT-hIAPP and R-hIAPP dimers and (B) rIAPP monomer and dimer. The percentage of each cluster is given below the structure in the figure.

In WT-hAIPP dimeric structures (a), (b), and (c) in Figure 7-(A), the two chains stand on opposite sides of each other (antiparallel), and the C-terminal of one chain is facing the N-terminal of the other chain. There is a probability that the first turn of the N-terminal helix (residues 2−3) opens and forms a β-strand with the C-terminal of the other chain (structure (a)). All the β-strands found in the clustering of WT-hIAPP are antiparallel.

2. hIAPP Dimer without a Disulfide Bridge. To explore the role of the Cys2−Cys7 disulfide bond in the structure of the smallest hIAPP aggregate dimer, we run HT-REMD simulations on R-hIAPP using the same parameters and time length as for WT-hIAPP. Entropy versus temperature plots averaged over various time intervals are given in Figure 1(B) . While the entropy evolves in the 400−700 ns interval, the last 200 ns interval is well converged, and the entropies averaged over 500−600 ns and 600−700 ns time intervals are the same. Similar to the WT-hIAPP dimer, we used the data generated in the last 200 ns of the simulation for analysis.

The secondary structure propensity for each residue at 300 K is shown in Figure 2(A) . The absence of the disulfide bond reduces the α-helical propensity by at least 75% in the N-terminal region, destabilizing completely the helix in the 1−9 region; residues 10−15 are now the only region with a notable α-helical propensity, about 20%. This allows the formation of a β structure spaning residues 5−9 in the N-terminal for R-hIAPP with a probability between 5 and 24%. While this new β-sheet region modifies slightly the β-strand propensity in the region 17−25, the overall secondary structure propensity of the C-terminal remains close to that of the wild-type sequence.

In agreement with the results for the hIAPP monomer, the presence of the disulfide bond restricts the formation of β structure for the N-terminal region and strongly induces α-helix formation (see Figure 2(A)). Contrary to WT-hIAPP, where the dimer increases the propensity of forming ordered secondary structure, the total α-helix and β-sheet contents for the R-hIAPP dimer is ∼18% at 300 K, significantly lower than the ∼28% observed at the same temperature for the R-hIAPP monomer[20] (Figure 2(C)). This is likely due to the increased probabilities of interchain interactions in the N-terminal region of R-hIAPP with respect to the wild-type sequence made possibly by the absence of an α-helix below residue Gln10. A comparison in the number of interchain contacts between WT-hIAPP and R-hIAPP in Figure 3 confirms that the main difference between the two sequences is found in the 1−9 region. Another difference in the contact probability map is observed in the region of residues 12−16, in which residues Leu12 and Phe16 have lower contact probability of ∼60% for R-hIAPP. In particular, Figure 4(B) shows a significant decrease in interchain contacts between Leu12−Ile26, Leu16−Ile26, and Leu16−Leu27 (average contacts at 300 K

dx.doi.org/10.1021/jp108870q |*J. Phys. Chem. B* 2011, 115, 3146–3154

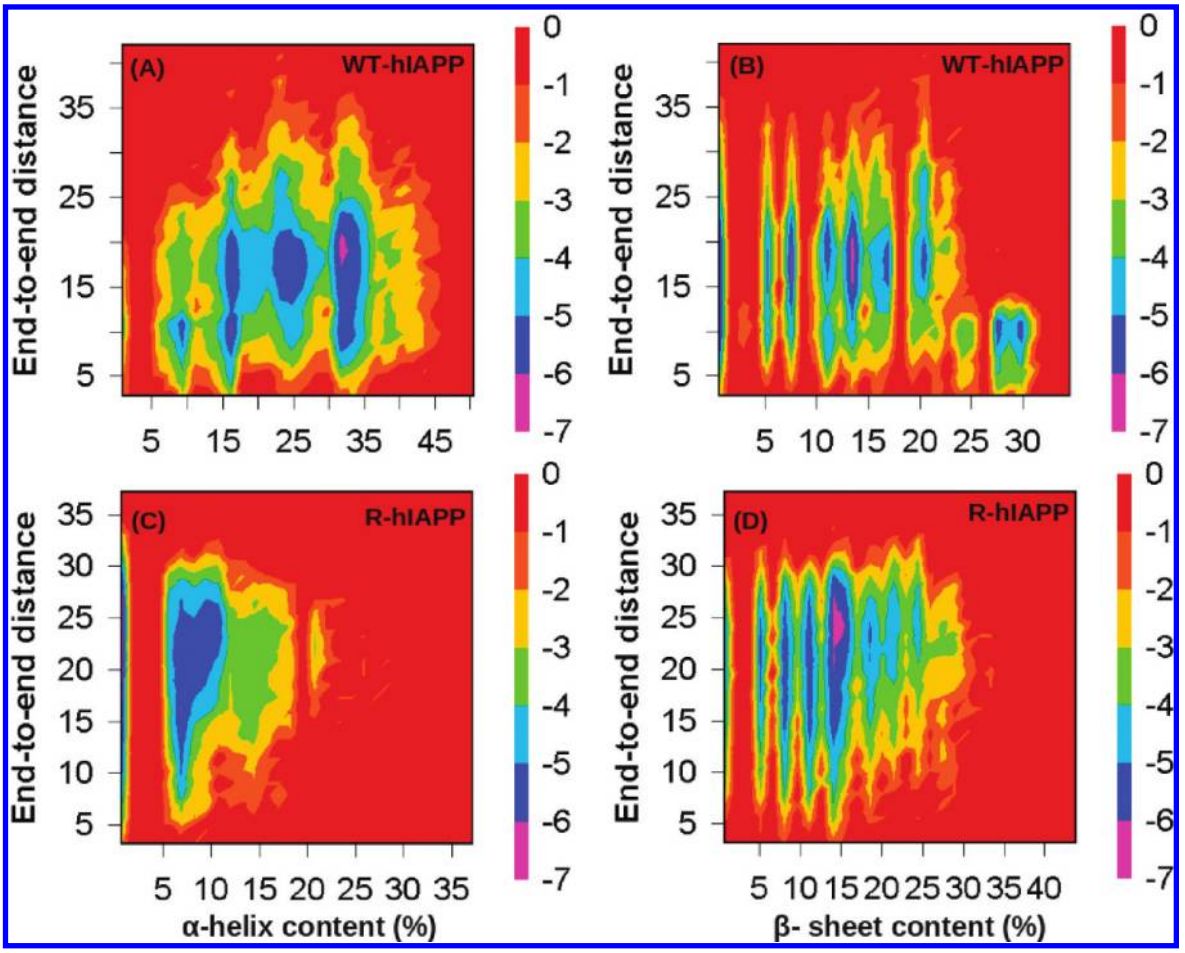

Figure 8. Free-energy landscape of WT-hIAPP and R-hIAPP at 300 K. (A) WT-hIAPP as a function of end-to-end distance and percentage of α-helix content. (B) For WT-hIAPP as a function of end-to-end distance and percentage of β-sheet content. (C) R-hIAPP as a function of end-to-end distance and percentage of α-helix content. (D) R-hIAPP as a function of end-to-end distance and percentage of β-sheet content.

between 62 and 76%) . More importantly, however, we also observe a very strong contact, with a probability above 90%, between C2−C7, while this contact is absent, of course, for WT-hIAPP. The amyloidogenic residues 20−27 region, for its part, is almost unaffected by the reduction of the disulfide bond, and interchain contacts between residues Ile26−Leu27 and Phe23−Leu27 are similar to the WT-hIAPP dimer. we also observe a very weak contact, with a probability below 10%, between Thr30 and Val32 in the C-terminal amyloidogenic region of residues 30−37, while this contact is stronger (with a probability of 28−35%) in WT-hIAPP .

This change in the interchain contact can also be observed in the clustering (Figure 7). The two chains interact strongly in the N-terminal region, preventing the formation of the longer α-helix observed for the monomer and leading instead to the appearance of a small and unstable β-sheet as the increasing temperature (around 260 K) destabilizes the short α-helices observed in both chains. From Figure 7(A), the structures (a), (b), and (c), in the R-hIAPP row, disappear through the transition at 260 K and form structure (d). This latter has lost almost all α-helix and β-sheet contents (corresponding to the small shoulder in the specific heat curve around 325 K) to become random coil at temperatures higher than 325 K .

We observe a similar trend between R-hIAPP and WT-hIAPP at all temperatures, as can be seen in in Figure 5 . Even at the lowest T, the α-helical propensity is 50% less than that of the wild-type, falling rapidly to a negligible value. Although β-content in R-hIAPP is higher at the lowest temperature (240 K), it rapidly destabilizes and follows exactly the same curve as WT-hIAPP above 275 K. We can understand this result by looking at the specific heat, where we observe a small transition near 260 K and a weak shoulder between 310 and 320 K. These very smooth structures in the specific heat are characteristic of a continuous disordering and an absence of marked secondary structure.

Free-energy landscape contour maps as a function of secondary structure and end-to-end distance are given in Figure 8 for both sequences at 300 K. WT-hIAPP displays four metastable structures as a function of α-helical content (panel (A)), indicating a number of competing families, while the corresponding free-energy landscape for R-hIAPP (panel (C)) reveals a single minimum at very low α-helical content. There is more similarity in terms of β-sheet content although (panels (B) and (D)), once again, we observe metastable minima at a higher fraction of secondary structure for the wild-type sequence (panel (B)). We observe, moreover, relatively low free-energy barriers between the three metastable minima at 16, 25, and 32% α-helical content for WT-hIAPP, indicating a high degree of plasticity that is not as present in the β-sheet contents, where barriers between local minima tend to be much steeper.

B. Rat IAPP. Simulations were run for the monomer and dimer of rIAPP with disulfide bridge using the same parameters as for the hIAPP systems. Because the number of visited structures is

dx.doi.org/10.1021/jp108870q |J. Phys. Chem. B 2011, 115, 3146–3154

much smaller than in the hIAPP systems, convergence is significantly faster for this sequence, and the simulation time is 400 ns for the monomer and 250 ns for the dimer of rIAPP to collect enough data for the analysis and to compare with the hIAPP results.

1. rIAPP Monomer. The runs for the rIAPP monomer reach equilibration quickly, as can be seen in Figure 1(C). The secondary structure percentage at 300 K in Figure 2(B) shows two regions with α-helix content: residues 5−16 and 29−34 with a maximum percentage of 96% and 38%, respectively, and no β-sheet content. The N-terminal region in rIAPP is very similar to hIAPP; however, due to the relative isolation of this region caused by the presence of the prolines, the observed α-helix percentage is higher than both types of hIAPP.

This structural simplicity is reflected in the specific heat, which shows a single transition at 320 K (Figure 6) associated with the α-helix melting, leading to fully random coil structure. The loss of helical structure in the rIAPP monomer with increasing temperature can be seen clearly in Figure 5(B) and in the dominant clusters at temperatures ranging from 240 to 300 K in Figure 7(B) .

2. rIAPP Dimer. The dimer of rIAPP also equilibrates rapidly as can be seen in Figure 1(C). Similar to the other systems, data are accumulated over the last 200 ns. The centers of the largest cluster in Figure 7(B) show the two chains each have two regions of α-helices connected with a turn compatible with the structure from NMR data.[28] The secondary structure percentage for the rIAPP monomer and dimer are identical: the probability profile in Figure 2(B) at 300 K shows two regions with α-helix content. The first region is the same as the WT-hIAPP dimer (see Figure 2(A)), residues 5−16, with a helix percentage of 95%, and the second region is from residues 29−35 with a maximum helix percentage of 40%. No β-sheet content is observed in the whole range of temperatures in the rIAPP dimer (see Figure 2(B)).

Figure 7(B) shows that at low temperature the N-terminal α-helices in the two chains are perpendicular to each other. After the first transition, however, they come into a parallel position, unlike the hIAPP in which the two chains are always antiparallel (see Figure 7(B).

The interchain contact map (Figure 4(C)) indicates high contact probability (between 40 and 85%) for L12−L16, F15−L16, L12−I26, L12−L27, L16−L27, I26−V32, and V32−L27. In contrast with WT-hIAPP, the amyloidogenic regions (residues 22−27 and 30−37) display very little interaction; for L27−I26, G24−F23, L27−F23, and I26−F23 the contacts drop to 6%−20%, and the contacts between Y37, F15, and F23 are less than 10% (see Figure 4(C)).

Overall, therefore, the mutations leading to the rIAPP sequence maintain the α-helical propensity in the N-terminal but destroy the amyloid-favorable β-sheet content observed in the C-terminal region of hIAPP.

IV. CONCLUSIONS

The structures of hIAPP dimer, in wild-type and reduced form, as well as those of the monomer and the dimer of rIAPP, have been investigated using HT-REMD simulations combined with the coarse-grained OPEP potential. Data obtained from our extensive simulations show a strong correlation between the presence/absence of the disulfide bond as well as amino acid sequence and their structural properties.

Previous simulations on the WT-hIAPP monomer have shown a strong α-helical propensity at residues 5−16 and a much weaker β-sheet between residues 22−26 and 30−35.[20] For identical sequences, the absence of a single disulfide bond increases the β-structure propensity in the C-terminal, especially at lower temperature, at the expense of the N-terminal α-helix.[20]

For both wild-type and reduced hIAPP dimers, the β-sheet is strongly stabilized by interchain contacts, indicating that the dimer formation is a significant step in the amyloidogenic process. The presence of dimer in the early stage of WT-hIAPP aggregation has been reported in a recent study using mass spectrometry.[48] More precisely, in the dimeric form of WT-hIAPP, we observe a very stable α-helix spanning residues 5−16, similar to that seen for the monomer, but followed, here, by significantly strengthened and expanded β-strands in the amyloidogenic region, between residues 17−27 and 29−35. Reduction of the Cys2−Cys7 disulfide bridge destabilizes much of the α-helix, which forms now in the 10−15 region, with a 20% probability only at 300 K, but leaves the C-terminal almost unaffected.

It has been proposed that early oligomerization of hIAPP is promoted by helix−helix association,[17] a suggestion recently supported by NMR spectroscopic results that show the N-terminal region (residues 1−17) could be responsible for the initial self-association of the WT-hIAPP peptide in bulk solution.[10] Our simulations suggest that some helix−helix interactions may exist in hIAPP in the presence of a disulfide bond as the WT-hIAPP dimer shows strong interchain hydrophobic interactions in the N-terminal region between the side chains of L12−F15 and L12−L16 which have 80% propensity to form an α-helix structure. This disulfide bond is essential for the formation of the N-terminal α-helix which, in turns, provides a support for the C-terminal β-sheet. The α-helical and β-sheet structures are significantly more stable below 300 K for the wild type than for the reduced sequence as is shown in Figure 5.

A tendency to form β-sheet is, of course, also necessary for oligomerization. Monomeric and dimeric rIAPP on the other hand, consistent with the experimental results,[28] display an α-helix in the N-terminal, with a distortion in the middle of the chain and followed by the second shorter α-helix without any β-sheet content. This is not so surprising, of course, as the three proline residues in the C-terminal are well-known β-breakers. Without β-strands, however, the β-sheet-rich dimer of rIAPP never forms. Structural comparison between rIAPP and hIAPP in Figure 7(A) and (B) suggests that β-sheet formation plays an important role in the early stage of hIAPP aggregation.

This study presents the conformational properties of the smallest aggregate−dimer occurring in the early steps of hIAPP aggregation and shows microscopic details in excellent agreement with several experimental data. It shows the very subtle role played by the Cys2−Cys7 disulfide bridge and indicates that, for this sequence, the dimer already contains the main structural elements necessary for fibril formation.

AUTHOR INFORMATION

Corresponding Author

*E-mail: rozita.laghaei@umontreal.ca or normand.mousseau@umontreal.ca.

ACKNOWLEDGMENT

N.M. acknowledges support from the Natural Sciences and Engineering Research Council of Canada and the Canada Research Chair Foundation. G.W. acknowledges the financial

support from the National Natural Science Foundation of China (11074047), the Program for New Century Excellent Talents in University (NCET-08-0125), and Research Fund for the Doctoral Program of Higher Education of China (RFDP). Calculations were done on the computers of the *Réseau québécois de calcul de haute performance*.

REFERENCES

(1) Clark, A.; Lewis, C. E.; Willis, A. C.; Cooper, G. J. S.; Morris, J. F.; Reid, K. B. M.; Turner, R. C. *Lancet* **1987**, *330*, 231.
(2) Höppener, J. W.; Lips, C. J. *Int. J. Biochem. Cell Biol.* **2006**, *38*, 726.
(3) Mirzabekov, T. A.; Lin, M. C.; Kagan, B. L. *J. Biol. Chem.* **1996**, *271*, 1988.
(4) Kayed, R.; Bernhagen, J.; Greenffeld, N.; Sweimeh, K.; Brunner, H.; Voelter, W.; Kapurniotu, A. *J. Mol. Biol.* **1999**, *287*, 781.
(5) Luca, S.; Yan, W.-M.; Leapman, R.; Tycko, R. *Biochemistry* **2007**, *46*, 13505.
(6) Wilzius, J. J.; Sievers, S. A.; Sawaya, M. R.; Cascio, D.; Popov, D.; Riekel, C.; Eisenberg, D. *Protein Sci.* **2008**, *18*, 1467.
(7) Brender, J. R.; Lee, E. L.; Cavitt, M. A.; Duncan, A. G.; Steel, G.; Ramamoorthy, A. *J. Am. Chem. Soc.* **2008**, *130*, 6424.
(8) Engel, M. F. M.; Khemtemourian, L.; Kleijer, C. C.; Meeldijk, H. J. D.; Jacobs, J.; Verkleij, A. J.; de Kruijff, B.; Killian, J. A.; Hoeppener, J. W. M. *Proc. Natl. Acad. Sci. U.S.A.* **2008**, *105*, 6033.
(9) Engel, M. F. *Chem. Phys. Lipids* **2009**, *160*, 1.
(10) Mishra, R.; Geyer, M.; Winter, R. *ChemBioChem* **2009**, *10*, 1769.
(11) Jiang, P.; Xu, W.; Mu, Y. *PLoS. Comput. Biol* **2009**, *5*, e1000357.
(12) Milardi, D.; Pappalardo, M.; Pannuzzo, M.; Grasso, D. M.; Rosa, C. L. *Chem. Phys. Lett.* **2008**, *463*, 396.
(13) Mo, Y.; Lu, Y.; Wei, G.; Derreumaux, P. *J. Chem. Phys.* **2009**, *130*, 125101.
(14) Friedman, R.; Pellarin, R.; Caisch, A. *J. Mol. Biol.* **2009**, *387*, 407.
(15) Rivera, E.; Straub, J.; Thirumalai, D. *Biophys. J.* **2009**, *96*, 4552.
(16) Apostolidou, M.; Jayasinghe, S. A.; Langen, R. *J. Biol. Chem.* **2008**, *283*, 17205.
(17) Abedini, A.; Raleigh, D. P. *Phys. Biol.* **2009**, *6*, 015005.
(18) Yonemoto, I. T.; Kroon, G. J. A.; Dyson, H. J.; Balch, W. E.; Kelly, J. W. *Biochemistry* **2008**, *47*, 9900.
(19) Cort, J. R.; Liu, Z.; Lee, G. M.; Huggins, K.; Janes, S.; Prickett, K.; Andersen, N. H. *Protein Eng., Des. Sel.* **2009**, *22*, 497.
(20) Laghaei, R.; Mousseau, N.; Wei, G. *J. Phys. Chem. B* **2010**, *114*, 7071–7077.
(21) Kajava, A. V.; Aebi, U.; Steven, A. C. *J. Mol. Biol.* **2005**, *348*, 247.
(22) Engel, M. F.; Yigittop, H.; Elgersma, R. C.; Rijkers, D. T. S.; Liskamp, R. M. J.; de Kruijff, B.; Hoppener, J. W. M.; Killian, J. A. *J. Mol. Biol.* **2006**, *356*, 783.
(23) Patil, S. M.; Xu, S.; Sheftic, S. R.; Alexandrescu, A. T. *J. Biol. Chem.* **2009**, *284*, 11982.
(24) Nielsen, J. T.; Bjerring, M.; Martin, R. O. P.; Jeppesen, D.; Pedersen, J. M.; Hein, K. L.; Vosegaard, T.; Skrydstrup, T.; Otzen, D. E.; Nielsen, N. C. *Angew. Chem., Int. Ed.* **2009**, *48*, 2118.
(25) Koo, B. W.; Miranker, A. D. *Protein Sci.* **2005**, *14*, 231.
(26) Goldsbury, C.; Goldie, K.; Pellaud, J.; Seelig, J.; Frey, P.; Kistler, S. A. M. J.; Cooper, G. J. S.; Aebi, U. *J. Struct. Biol.* **2000**, *130*, 352.
(27) Williamson, J. A.; Miranker, A. D. *Protein Sci.* **2007**, *16*, 110.
(28) Nanga, R. P. R.; Brender, J. R.; Xu, J.; Hartman, K.; Subramanian, V.; Ramamoorthy, A. *J. Am. Chem. Soc.* **2009**, *131*, 8252.
(29) Nanga, R. P. R.; Brender, J. R.; Xu, J.; Hartman, K.; Veglia, G.; Ramamoorthy, A. *Biochemistry* **2008**, *47*, 12689.
(30) Brender, J. R.; Hartman, K.; Reid, K. R.; Kennedy, R. T.; Ramamoorthy, A. *Biochemistry* **2008**, *47*, 12680.
(31) Sugita, Y.; Okamoto, Y. *Chem. Phys. Lett.* **1999**, *314*, 141.
(32) Maupetit, J.; Tuffery, P.; Derreumaux, P. *Proteins: Struct., Funct., Bioinf.* **2007**, *69*, 394.
(33) Derreumaux, P. *J. Chem. Phys.* **1999**, *111*, 2301.
(34) Maupetit, J.; Derreumaux, P.; Tuffery, P. *Nucleic Acids Res.* **2009**, *37*, W498.
(35) Wei, G.; Song, W.; Derreumaux, P.; Mousseau, N. *Front. Biosci.* **2008**, *13*, 5681.
(36) Lu, Y.; Derreumaux, P.; Guo, Z.; Mousseau, N.; Wei, G. *Proteins* **2009**, *75*, 954.
(37) Chebaro, Y.; Dong, X.; Laghaei, R.; Derreumaux, P.; Mousseau, N. *J. Phys. Chem. B* **2009**, *113*, 267.
(38) Chebaro, Y.; Mousseau, N.; Derreumaux, P. *J. Phys. Chem. B* **2009**, *113*, 7668.
(39) Laghaei, R.; Mousseau, N. *J. Chem. Phys.* **2010**, *132*, 165102.
(40) Faraldo-Gomez, J. D.; Roux, B. *J. Comput. Chem.* **2007**, *28*, 1634.
(41) Berendsen, H.; Postma, J.; van Gunsteren, W.; Nola, A. D.; Haak, J. *J. Chem. Phys.* **1984**, *81*, 3684.
(42) Andersen, H. C. *J. Comput. Phys.* **1983**, *52*, 26.
(43) Chodera, J. D.; Swope, W. C.; Pitera, J. W.; Seok, C.; Dill, K. A. *J. Chem. Theory Comput.* **2007**, *3*, 26.
(44) Frishman, D.; Argos, P. *Proteins* **1995**, *23*, 566.
(45) Daura, X.; Gademann, K.; Jaun, B.; Seebach, D.; van Gunsteren, W. F.; Mark, A. E. *Angew. Chem., Int. Ed. Engl.* **1999**, *38*, 236.
(46) Nilsson, M. R.; Raleigh, D. P. *J. Biol. Chem.* **1999**, *294*, 1375.
(47) Padrick, S. B.; Miranker, A. D. *J. Mol. Biol.* **2001**, *308*, 783.
(48) Wei, L.; Jiang, P.; Xu, W.; Li, H.; Zhang, H.; Yan, L.; Chan-Park, M. B.; Liu, X.-W.; Tang, K.; Mu, Y.; et al. *J. Biol. Chem.* **2011**in press.